

MMPTRACK: Large-scale Densely Annotated Multi-camera Multiple People Tracking Benchmark

Xiaotian Han, Quanzeng You, Chunyu Wang, Zhizheng Zhang, Peng Chu,
Houdong Hu, Jiang Wang, Zicheng Liu
Microsoft

{xiaothan, quyou, chnuwa, zhizzhang, pengchu, houhu, jiangwang, zliu}@microsoft.com

Abstract

Multi-camera tracking systems are gaining popularity in applications that demand high-quality tracking results, such as frictionless checkout because monocular multi-object tracking (MOT) systems often fail in cluttered and crowded environments due to occlusion. Multiple highly overlapped cameras can significantly alleviate the problem by recovering partial 3D information. However, the cost of creating a high-quality multi-camera tracking dataset with diverse camera settings and backgrounds has limited the dataset scale in this domain. In this paper, we provide a large-scale densely-labeled multi-camera tracking dataset in five different environments with the help of an auto-annotation system. The system uses overlapped and calibrated depth and RGB cameras to build a high-performance 3D tracker that automatically generates the 3D tracking results. The 3D tracking results are projected to each RGB camera view using camera parameters to create 2D tracking results. Then, we manually check and correct the 3D tracking results to ensure the label quality, which is much cheaper than fully manual annotation. We have conducted extensive experiments using two real-time multi-camera trackers and a person re-identification (ReID) model with different settings. This dataset provides a more reliable benchmark of multi-camera, multi-object tracking systems in cluttered and crowded environments. Also, our results demonstrate that adapting the trackers and ReID models on this dataset significantly improves their performance. Our dataset will be publicly released upon the acceptance of this work.

1. Introduction

Multiple object tracking (MOT) [7, 31] is one of the fundamental research topics in computer vision. As more efficient and powerful deep neural networks are continuously being developed, the accuracy of MOT systems has been improved a lot in recent years. However, monocular

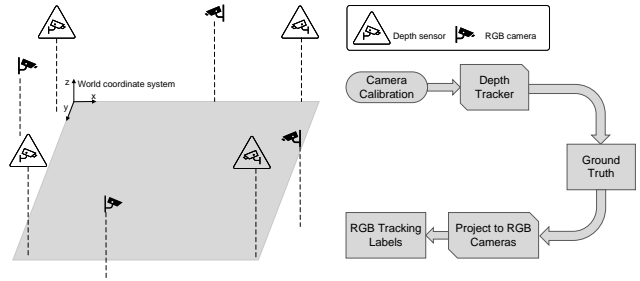


Figure 1. Illustration of our auto-annotation system. We have multiple calibrated depth sensors and RGB cameras installed in an environment. We build a high-performance 3D tracker to generate pseudo ground-truth tracking results in 3D space. These tracking results are projected to each RGB camera view as multi-camera multiple people tracking labels.

lar MOT systems still face severe challenges in cluttered and crowded environments, where occlusions of the tracked objects often occur. Thus, their accuracies are inadequate for applications that require highly accurate and consistent tracking results, such as frictionless checkout in retail stores or autonomous driving.

Recently, multi-camera systems have been widely deployed in these applications [1]. The overlapped and calibrated cameras can considerably remedy the occlusion issue, and have achieved much higher accuracy than single-camera tracking systems [48]. However, we only have a few small multi-camera datasets publicly available due to data collection and annotation challenges. The lack of high-quality training and evaluation data makes it difficult to understand the challenges and improve the current multi-camera tracking systems.

In this paper, we propose a large-scale multi-camera multi-object tracking dataset, which is collected and annotated by an auto-annotation system. Figure 1 illustrates the overview of the auto-annotation system. It consists of multiple calibrated depth sensors and RGB cameras. In particular, we follow the design in [44], where the depth tracker works on the projected top-down view of the 3D

space. We train a top-down person detector on the projected view and follow the tracking-by-detection framework [3] to build a high-quality tracker on the projected view. The 3D tracker can produce consistent and accurate tracking results on the projected top-down view. We use human annotators to correct the 3D tracking errors, such as ID switches and false-positive tracks. The corrected per-frame 3D tracking results are projected to all synchronized RGB streams using the camera parameters. Our experiments show that the auto-annotation system can produce very high quality tracking annotations (100% IDf1 and 99.9% MOTA) using only 1/800 of the cost of the traditional annotation methods.

We set up five diverse and challenging environments equipped with the auto-annotation system in our lab. With the help of the auto-annotation system, we construct the largest multi-camera multiple people tracking dataset so far. The dataset is densely annotated, *e.g.*, per-frame bounding boxes and person identities are available.

We evaluate two state-of-the-art real-time multi-camera person trackers [45, 48] and a person re-identification (ReID) model [50] on this dataset under various settings. Although the state-of-the-art multi-camera tracking systems perform much better than single-camera tracking systems, we find that their performance is still below the requirements of demanding applications. In addition, the detectors, trackers, or Re-ID models trained on publicly available datasets, such as MS-COCO [29] or MSMT [40], are not performing well in these challenging environments because of large viewpoint and domain gap. Adapting the models using the training split of the data can significantly improve the accuracy of the system. We expect the availability of such large-scale multi-camera multiple people tracking dataset will encourage more participants in this research topic. This dataset is also valuable for the evaluation of other tasks, such as multi-view people detection [20, 28] and monocular multiple people tracking [7]. To summarize, our contributions are as follows:

- We construct the largest densely annotated multi-camera multiple people tracking dataset to encourage more research on this topic.
- We propose an auto-annotation system, which can produce high-quality tracking labels for multi-camera environments in a fast and cost-efficient way.
- We conduct extensive experiments to reveal the challenges and characteristics of our dataset.

2. Related work

Approaches Multi-camera multi-object tracking has been extensively studied in the computer vision community. Previously, different graph-based approaches have been proposed to solve the data associations across different frames

and cameras [5, 11, 12, 17, 18, 35, 38, 41, 46]. Recent approaches [22, 33, 37, 43] attempt to apply deep ReID features for the data association. Extra efforts are needed to handle cross-camera appearance changes [21, 23]. These methods can be applied to environments with non-overlapping cameras, but they cannot explicitly utilize the camera calibration information for cross-camera data association and 3D space localization.

Other approaches adopt camera calibration for tracklets merging and cross-camera association. Probabilistic occupancy map (POM) [15] is one of the early representative studies. POM provides a robust estimation of the ground-plane occupancy, which is the key to building a high-performance tracker in crowded environments. Also, homography [13] is employed to merge head segmentations from all camera views to build a head tracker. Later, deep occlusion [4] extends this idea by utilizing Convolutional Neural Network (CNN) and Conditional Random Field (CRF) to reason the occlusions.

Recently, 3D pose estimation and 3D person detection are also utilized for multi-camera person tracking [48]. 3D pose can be estimated [10, 36] by merging 2D skeleton estimations from multiple 2D camera views, using a 3D regression network or graph matching. Meanwhile, multi-view person detection approaches [19, 20, 28, 34] also utilize camera calibration to merge multiple 2D detections or features to generate more reliable 3D person detection results. The accuracy of these approaches heavily depends on the quality of the 2D person detection or 2D pose estimation. These 3D poses and detections can be utilized for 3D trackers.

Datasets Several multi-camera tracking datasets with highly overlapping cameras, have been widely adopted in multi-target multi-camera tracking research. Among them, PETS2009 [14], Laboratory [15], Terrace [15], Passage-way [15], USC Campus [25] and CamNet [47] have been collected with low-resolution cameras and these datasets only have a limited number of frames and person identities (IDs). EPFL-RLC [9], CAMPUS [42] and SALSA [2] are released more recently. However, EPFL-RLC only has 300 fully annotated frames, and CAMPUS comes without 3D ground truth. WILDTRACK dataset [8] consists

Dataset	# of Envs	Cameras	FPS	Overlap	Calib	GT (frames)	Length (minutes)
USC Campus [25]	1	3	30	No	No	135,000	25
CamNet [47]	6	8	25	Yes	No	360,000	30
DukeMTMC [32]	1	8	60	No	Yes	2,448,000	85
SALSA [2]	1	4	15	Yes	Yes	~1,200	60
WILDTRACK [8]	1	7	60	Yes	Yes	~7×9,518	60
MMPTRACK (ours)	5	23	15	Yes	Yes	~2,979,900	576

Table 1. Representative multi-camera person tracking datasets. FPS stands for frame per second.

of high-quality annotations of both camera-view and 3D ground truth, as well as more person identities. However, the annotations are sparse and limited to 400 frames. DukeMTMC [32] is released with over 2 million frames and more than 2700 identities. However, there are almost no overlaps between different cameras. Table 1 compares our dataset (MMPTRACK) with several existing datasets. MMPTRACK is captured with a large number of calibrated overlapping cameras in indoor environments, which aligns better with the applications such as frictionless checkout. MMPTRACK is much larger than the existing data both in terms of the video length and the number of annotated frames. The videos are densely labeled with per-frame tracking bounding boxes and person identities.

3. Dataset collection

This section gives a detailed overview of how we collect our dataset, including environment setup, camera calibration procedure, and annotation pipeline.

3.1. Dataset statistics

Envs	Retail	Lobby	Industry	Cafe	Office	Total
# of cameras	6	4	4	4	5	23
Train (min)	84	65	52	14	46	261
Validation (min)	43	32	31	28	19	153
Test (min)	45	32	32	31	22	162
Total (min)	172	129	115	73	87	576

Table 2. Statistics of Multi-camera Multiple People Tracking (MMPTRACK) dataset.

The detailed statistics are summarized in Table 2. Our dataset is recorded with 15 frames per second (FPS) in five diverse and challenging environment settings. With the help of our auto-annotation system, we can obtain the per-frame tracking bounding box labels in the collected videos efficiently. Overall, we collect about 9.6 hours of videos, with over half a million frame-wise annotations for each camera view. This is by far the largest publicly available multi-camera multiple people tracking (MMPTRACK) dataset.

Figure 2 shows some examples of the tracking labels of each camera view from two different environments. Although both environments are crowded and cluttered, our ground truth consists of high-quality bounding boxes and consistent person IDs across all camera views.

3.2. Environment setup

We set up 5 different environments in our lab, *i.e.*, *Cafe Shop*, *Industry*, *Lobby*, *Office* and *Retail*. We install Azure Kinect cameras in each of these environments with fixed positions and camera angles. Figure 3 shows the field

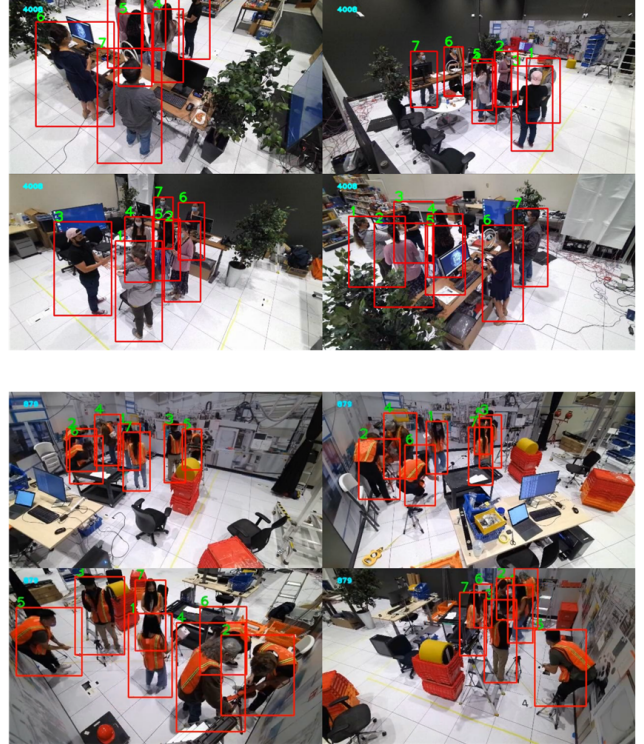


Figure 2. Examples of the images and tracking labels of our dataset. **Above**: images and labels of four camera views in *Lobby* environment. **Below**: images and labels of four camera views in *Industry* environment.

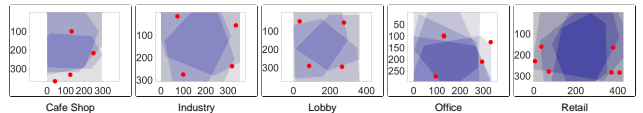


Figure 3. Field of view overlaps of different cameras in different environments on the ground plane. Each red dot represents the location of a camera. The X and Y axes represent the size of each environment in terms of pixels (each pixel unit is 20mm).

of views overlaps among different cameras on the ground plane. Azure Kinects can record RGB and depth streams simultaneously. Azure Kinects' RGB streams will be used as the default RGB cameras for our dataset (see Figure 1)¹. The depth and RGB streams of all Azure Kinects are all recorded and time-synchronized.

3.3. Camera calibration

Intrinsic parameters We obtain Azure Kinect intrinsic parameters directly from its SDK. We denote intrinsic parameters as I .

Extrinsic parameters In our settings, one camera has the overlapping field of views with at least another camera. We

¹With multiple camera calibrations, 3D tracking labels can be projected to other types of RGB cameras.

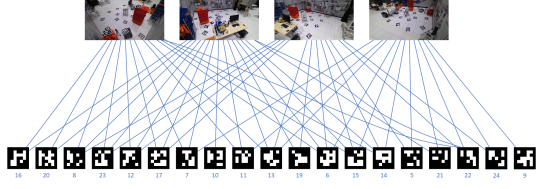


Figure 4. Example of bipartite graph from cameras and ArUco markers. The above 4 cameras are from Industry environment.

use ArUco markers as reference points in the world coordinate system. We build a connected bipartite graph, where cameras and ArUco markers are vertices. If ArUco marker m_i is within the view of camera c_j , we will add an edge e_{ij} between them. Figure 4 shows an example of the connected bipartite graph when we calibrate the *Industry* environment. Let $P = \bigcup P_i$ be the set of detected corner points of all markers (P_i is the corners from i -th marker). Then, the set of extrinsic parameters E is obtained by optimizing

$$E^* = \arg \max_{E, M} \sum_{i=1}^{|P|} \sum_{c=1}^C \mathbb{1}_i^c \|p_i^c - I^c * E^c * m_i\|^2, \quad (1)$$

where $\|\cdot\|$ denotes Euclidean distance, $\mathbb{1}_i^c$ is an indicator function, whose value equals to 1 only if point p_i is visible in camera view c , $M = \{m_i, i = 1, \dots, |P|\}$ denotes the markers' corner points in world coordinate system. The graph optimization approach proposed in [26] is implemented to solve Eq. (1).

3.4. Dataset collection

The current dataset is recorded in four half-day sessions. In each session, we hire seven different subjects to participate. The actors can act improvisationally as long as their action fits the environment setting. For instance, in *Retail* environment, they are free to perform any shopping behaviors, e.g., pushing shopping carts, holding baskets, and standing in a queue for checkout. Following such instructions, we believe the collected dataset covers a wide variety of behaviors. In total, we have 28 subjects, with different ages, genders, and ethics, who participated in the data collection (see Table 2 for the statistics of our dataset).

3.5. 3D auto-annotation system

Our 3D auto-annotation system utilizes depth streams to track multiple people with high accuracy. The overall workflow of the system is described in Algorithm 1. We build our 3D tracker using data released in [44], which does not have any overlap with the current dataset in terms of environment or subject. The top-down view image is constructed from the merged 3D point cloud. This design avoids environment-dependent factors, such as lighting, camera angles, etc. Therefore, the 3D tracker can be easily generalized and applied to different environments.

Algorithm 1 Workflow of RGBD Auto-annotation System

Input: Synchronized RGB and depth streams and camera parameters C

Output: Person bounding boxes and IDs in each camera view

```

procedure AUTO-ANNOTATION
   $B \leftarrow \text{list}()$  ▷ Person bounding boxes
  while All Streams not end do
     $R \leftarrow \text{set}()$  ▷ Synchronized RGB images
     $D \leftarrow \text{set}()$  ▷ Synchronized Depth images
    for stream in Streams do
       $r, d \leftarrow \text{stream.read}()$ 
       $\text{add}(r, R)$ 
       $\text{add}(d, D)$ 
    end for
     $P \leftarrow \text{PointCloudGen}(R, D, C)$ 
     $T_d \leftarrow \text{TopdownViewGen}(P)$  ▷ Top-down view of the scene
     $B \leftarrow \text{PersonDetector}(T_d)$ 
     $T_r \leftarrow \text{3DTracker}(B, P)$  ▷ 3D Tracklets
     $B_c \leftarrow \text{Projection}(T_r, C)$  ▷ Camera-view bounding boxes
     $\text{append}(B_c, B)$ 
  end while
  return  $B$ 
end procedure

```

Point cloud reconstruction We reconstruct the point cloud of the whole scene from calibrated and synchronized depth cameras. Given the intrinsic parameters I and extrinsic parameters E , the point cloud \mathbb{P} is calculated as follows:

$$\mathbb{P} = \bigcup_{c=1}^C \bigcup_i \bigcup_j (E^c)^{-1} * (I^c)^{-1} * [i, j, d_{i,j}^c]^T \quad (2)$$

where i and j index over all valid locations and $d_{i,j}^c$ denotes camera c 's depth measurement at location (i, j) .

Top-down view projection We discretize the point cloud \mathbb{P} into a binary voxel set \mathbb{V} . Each voxel $\mathbb{V}_{i,j,k}$ covers a cube with a volume of $20\text{mm} \times 20\text{mm} \times 20\text{mm}$. $\mathbb{V}_{i,j,k} = 1$ if and only if there exists at least one point $\mathbb{P}_{i',j',k'}$, such that it locates inside the cube covered by $\mathbb{V}_{i,j,k}$.

We set the world-coordinate system's X and Y axes parallel to the ground plane and the Z axis vertical to the ground. The top-down view image T_d can be obtained by projecting \mathbb{V} onto the X-Y ground plane. More specifically, its value at position (m, n) is computed as:

$$T_d(m, n) = \arg \max_{z, V(m,n,z)=1} \mathbb{V}_{m,n,z}, \quad (3)$$

which can be perceived as the *height* of filled voxels within each cube $V_{m,n}(\cdot)$.

Top-down view person detection We design a simple two-stage top-down person detector. We assume that each person center is roughly the highest point around a local region. Recall that pixel values of T_d (Eq. (3)) represent the height of each location. Therefore, in the proposal generation stage, we extract all local maxima from the top-down view image T_d . For each candidate position (i, j) , we crop a 20×20 square region centered around it. The cropped

Envs	IDF1↑	MOTA↑	FP↓	FN↓	IDs↓
Cafe	100	100	0	0	0
Industry	100	100	0	0	0
Lobby	100	100	0	0	0
Office	100	100	0	0	0
Retail	100	99.9	0	4	0

Table 3. Performance of our 3D tracker on one testing sequence.

image region is fed into a Convolutional Neural Network, which serves as a person classifier in the second stage.

3D tracker We develop a highly efficient 3D association method. The inputs of our method are top-down view detection boxes with corresponding detection scores and point clouds. We initialize a tracklet with a detection box whose score is above a threshold at the beginning stage. Then, for the following frames, we construct the cost matrix based on spatial and appearance (color histogram) distance between each tracklet and the detected bounding boxes. Association results are obtained by employing Hungarian Matching algorithm. For each unmatched detection bounding box, we generate a new candidate tracklet.

Camera-view projection The height h of each tracked person can be estimated from the local maxima of its top-down bounding box (each pixel value unit represents $20mm$). We fit a cube with a size of $100cm \times 100cm \times h$ bottom centered at each top-down tracked person. A 3D bounding box (cube) is projected to each camera view. The 2D bounding box in each view is the tightest rectangle that encloses the projected 3D bounding box in this view. In this way, we propagate the tracking results from 3D space to all RGB cameras within the same environment.

3.6. Annotation and quality control

The 3D tracker may still introduce errors occasionally. We manually fix all tracking errors before propagating the results to each RGB camera view. The most common errors in our RGBD Tracker are tracklet ID switch and false-positive person detection. We request annotators to correct ID switches and remove false-positive tracklets from 3D tracking results. Notice this process is relatively cost-efficient because no bounding box labeling is required, and all the corrections are performed at the tracklet level.

Based on our experience, each annotator can label around 600 frames (including boxes and IDs) per day for videos with around 5 to 6 persons inside. Manually labeling all the videos in our dataset costs 414 labeler days when we annotate every ten frames and interpolate the tracking labels to the remaining frames. Labeling all the frames costs more than 4000 labeler days. In comparison, we only need one labeler to work less than 5 hours to correct all the errors of our 3D tracker.

To test the quality of the 3D tracking ground truth, we sample 1,000 continuous frames from each environment

and manually label all the bounding boxes and ids of each tracklet. Table 3 summarizes the evaluation results of our corrected 3D tracker’s results using human-labeled ground truth. Only four human-labeled targets are not matched by our 3D tracking results, which is tolerable given that humans can also make errors.

4. Benchmarks

In this section, we discuss the evaluation metrics, evaluated approaches and experimental results on both *tracking* and *ReID* tasks.

4.1. Evaluation metrics

For the tracking task, we follow the widely adopted MOT metrics to evaluate the performance [7]. We report the false positive (FP) and false negative (FN) detections, which are also considered in multiple object tracking accuracy (MOTA). MOTA further deals with identity switches (IDs) and is extensively used in benchmarking different trackers. Besides, we also report **IDF1**, which measures the ID consistency between the predicted trajectories and the ground truth using ID precision and ID recall. IDF1 can assess the trackers’ ability on tracklet association. We report all performance metrics on the top-down view for multi-camera tracking, using the 3D ground-truth tracking results. We follow the settings in [8], where a radius of one meter is used as the distance threshold when computing all metrics.

For the ReID task, we adopt the widely used Rank-1 accuracy (R-1) and mean Average Precision (mAP) [50] to compare the model’s performance under different settings.

4.2. Evaluation approaches

4.2.1 Baselines trackers

We evaluate two state-of-the-art online real-time multi-camera trackers on our datasets. We focus on evaluating online real-time trackers because they can better reflect the core detection and tracking performance, and we can better observe the challenges in our dataset in these evaluations.

End-to-end deep multi-camera tracker (DMCT) In this baseline, we employ the end-to-end approach (DMCT) proposed in [45]. This approach estimates the ground point heatmap of each candidate at each camera view, projects the ground point heatmaps from all camera views to the ground plane, and fuses all the heatmaps into a ground-plane heatmap. Similar to [45], we train a variant of CornerNet [27] with pixel-wise Focal Loss [27] as our ground-point estimation model. The tracker works on the fused ground-plane heatmap.

Given the fused ground-plane heatmap H , two different approaches are utilized to obtain top-down person detections. The first approach is rule-based. It directly applies Gaussian blur to H and extracts local maxima as person

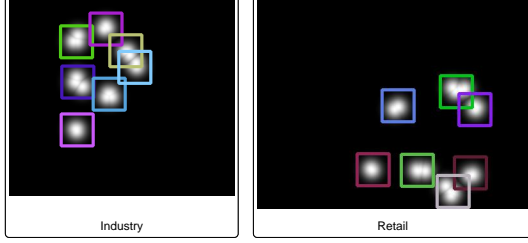


Figure 5. Examples of the fused ground-plane images as inputs to person detector. The bounding boxes are the ground truth.

detections for tracking. In this approach, The heatmaps $\{H_1, H_2, \dots, H_C\}$ from C camera views are projected to the ground plane using homographies between the ground plane and all camera views. For each location in fused top-down heatmap H , its value is the maximum over all camera view’s projected heatmap.

The second approach trains a YOLOV5 [24] detector as top-down person detector. The second approach is more expensive than the first approach, but it is much cheaper than the sequence-based deep glimpse network in [45]. In this approach, we first find the local maxima at each camera-view heatmap H_i as candidate points. These points are projected to the ground plane, and each point generates a Gaussian distribution around it to reduce noise. We keep the maximum value from all Gaussian distributions for each location in the projected top-down image. Figure 5 shows two examples of fused ground-plane heatmaps from two different environments. Although the two environments are configured with different RGB camera settings and backgrounds, the top-down images look similar. Our experimental results will show that the top-down detector can easily generalize across different environments.

We also label another external dataset using images from OpenImage². Specifically, we sample a subset of OpenImage containing persons, which has about 600,000 images. We manually label the ground point of each person in these images. In our experiments, we evaluate the impact of this external data on tracking performance.

The variants of DMCT approach include: **DMCT** train the ground-point estimation model on the training split of MMPTRACK and the rule-based approach for top-down person detection; **DMCT-TD** uses the same ground-point estimation model with DMCT and the deep learning-based top-down person detector; **DMCT-Ext** uses the same rule-based top-down person detection with DMCT, and it trains ground-point estimation model with both training split of MMPTRACK and the extra manually labeled OpenImage dataset; **DMCT-Ext-TD** uses the same ground-point estimation model with DMCT-Ext, and the deep learning-based top-down person detector.

²<https://storage.googleapis.com/openimages/web/index.html>

Tracking by 3D skeletons (VoxelTrack) This baseline performs tracking with estimated 3D body joints, which have more spatial information than the single ground point. It is built on top of a state-of-the-art 3D pose estimation method VoxelPose [36]. It requires neither camera-view 2D pose estimation nor cross-camera pose association as in previous works, which is error-prone. Instead, all hard decisions are postponed and made in the 3D space after fusing 2D visual features from all views, which effectively avoids error accumulation. In addition, the fused representation is robust to occlusion. A joint occluded in one camera view may be visible in other camera views.

We follow a standard pipeline [49] for tracking the 3D poses. We initialize every estimated 3D pose as a tracklet. For the following frames, we use the Hungarian algorithm to assign the 3D poses to the existing tracklets, where the matching cost is the sum of the 3D distance for all the 3D joints. We reject the assignment if the spatial distance between the tracklet and the 3D pose is too large. An unmatched 3D pose will be assigned to a new tracklet. An existing tracklet will be removed if it is not matched to any 3D poses for more than 30 frames.

Following the settings of [36], the 2D heatmap estimation model is trained on the COCO dataset, and the 3D models are trained using synthetic data. Since MMPTRACK lacks 3D pose labels, we conduct a *virtual* fine-tuning for the 3D models. Calibration parameters of MMPTRACK are employed to generate pseudo-3D human poses.

4.2.2 Baseline ReID models

We evaluate an advanced person re-identification (ReID) model proposed in FastReID [16] on the MMPTRACK dataset. The robust ReID feature can improve the performance of an MOT system. We study the challenges of learning discriminative ReID features in a cluttered and crowded environment under multiple cameras. Our baseline model is built upon a commonly used baseline model [30]. We further incorporate Non-local block [39], GeM pooling [6] and a series of training strategies (see details in [16]).

We uniformly downsample the MMPTRACK dataset with a step size of 32. During testing, we divide each downsampled sequence into two halves. We use the cropped persons in the first half as the query set and those in the second half as the gallery set. Although there are only a small number of person identities in this dataset, the diverse camera angles and cluttered backgrounds still make ReID a challenging task on our dataset.

We evaluate three training configurations of the above model on the testing split of MMPTRACK. Specifically, for the **Generalization** setting, we directly evaluate the model trained with the person ReID dataset MSMT [40]. For the **Adaptation** setting, we perform supervised fine-tuning of the previous model with cropped persons on the training

split of MMPTRACK. For the **Supervised** setting, we train the person ReID model from scratch using only the cropped persons in the training split of MMPTRACK.

4.3. Benchmark results and discussions

4.3.1 Tracking performance on MMPTRACK

We evaluate the two real-time baseline trackers on the collected MMPTRACK dataset.

Method	IDF1↑	MOTA↑	FP↓	FN↓	IDs↓
VoxelTrack	55.2	79.6	43,776	110,239	4,365
DMCT	60.2	91.5	34,450	41,920	2,158
DMCT-TD	74.8	93.6	15,080	42,854	620
DMCT-Ext	61.1	92.5	30,789	36,631	1,953
DMCT-Ext-TD	77.5	94.8	19,235	28,505	567

Table 4. Tracking performance on validation split.

Method	IDF1↑	MOTA↑	FP↓	FN↓	IDs↓
VoxelTrack	50.8	76.8	49,881	142,380	4,922
DMCT	56.0	88.8	39,715	52,559	2,677
DMCT-TD	68.1	93.2	16,023	40,606	935
DMCT-Ext	56.6	89.0	42,413	48,039	3,013
DMCT-Ext-TD	74.1	94.6	7,005	38,296	641

Table 5. Tracking performance on testing split.

Table 4 and Table 5 include the results of different baseline trackers on the validation and testing splits of our dataset respectively. The results suggest that the top-down person detector trained with a deep learning model can significantly boost the performance of baseline DMCT, especially for **IDF1** and **IDs**. With an extra of 600,000 images from OpenImage, **DMCT-Ext** shows slight improvements over **DMCT** in terms of **IDF1** and **MOTA**. **DMCT-Ext-TD** improves **IDF1** by 2.7 over **DMCT-TD**. However, the **MOTA** only increases 1.1. Compared with **VoxelTrack**, which is only virtually fine-tuned on MMPTRACK, all variants of **DMCT** perform better. We believe the performance gap is due to the large domain differences of our dataset and other public datasets such as MS-COCO, on which the **VoxelTrack** is trained. Since we can easily generate a large-scale multi-camera multi-object tracking dataset for an environment using our auto-annotation system, we can train a model that adapts to a given environment with improved accuracy. However, the accuracy of the baseline methods is still not high enough to meet the requirements of demanding applications, particularly for **IDF1**. Further research is needed in this domain.

Ablation studies We study the impact of different training splits on our baselines’ performance. Since **VoxelTrack** can only be virtually fine-tuned on our dataset, we only cover the ablation study results of different variants of **DMCT**. We attempt to study the impact of environment-specific data. In particular, we train the ground point estimation models and the top-down detectors with and without

each environment-specific data. Then, we report the performance in each environment individually.

Table 6 shows the tracking evaluation metrics without the top-down detector. Generally, without each environment’s data, the tracking performance drops significantly. This is particularly true in terms of the **IDF1** metric. Also, external training data can improve the tracker’s performance for most environments when environment-specific data is absent. However, with environment-specific data, external data leads to a limited performance gain.

Table 7 further studies **DMCT**’s performance when equipped with a deep learning-based top-down detector. A tracker with a deep learning-based top-down detector has better generability. Without external data, models trained with environment-specific data show better performance in *Industry* and *Retail* in terms of **IDF1**. However, models trained without environment-specific data even show better **IDF1** in *Cafe*, *Lobby* and *Office*. Also, when extra OpenImage data is utilized to train a ground point estimation model, the performance gain is limited, and in some environments, even worse than the results without the external data. It is generally believed that a pre-trained model on external data may provide good initialization when training the deep model. However, the domain gap between MMPTRACK and OpenImage makes the pre-training step insignificant. Instead, the large-scale in-domain MMPTRACK dataset can train a model with better performance. Meanwhile, compared with Table 6, the results in Table 7 also suggests that the deep-learning-based top-down detector reduces the performance gap caused by external ground-point data.

4.3.2 ReID performance on MMPTRACK

We report the results of the ReID model with the three different settings discussed in Section 4.2.2. The MSMT ReID dataset, which is employed to pretrain our **Generalization** and **Adaptation** model, consists of more than 4,000 indoor and outdoor person identities. The evaluation results are summarized in Table 8. Even though our training dataset consists of only 14 different person identities, training from scratch still outperforms the **Generalization** model. Notice that the person identities do not overlap in training and testing split. This shows that our large-scale dataset can help learn discriminative ReID features. Also, the fine-tuned model (**Adaptation** model) is superior to the model trained from scratch (**Supervised** model). Meanwhile, the performance of all models varies across different environments. All models perform poorly in *Retail* environment due to its cluttered background. In general, the experiment shows that Re-ID is very challenging in cluttered and crowded environments in multi-camera settings. Our large-scale dataset can help learn a more discriminative Re-ID feature that is adapted to a given environment. However, the performance

Method	w/Env Training	Env	Without external data					With external data				
			IDF1↑	MOTA↑	FP↓	FN↓	IDs↓	IDF1↑	MOTA↑	FP↓	FN↓	IDs↓
DMCT	✗	Cafe	39.4	87.7	12,012	7,589	1,158	56.9	91.8	6,792	6,382	701
DMCT	✓	Cafe	64.2	95.9	2,691	4,063	162	61.3	96.0	2,104	4,409	297
DMCT	✗	Industry	34.2	78.4	18,486	20,548	1,637	42.7	82.7	11,700	19,858	962
DMCT	✓	Industry	61.7	90.5	9,107	8,431	306	64.5	91.2	9,188	7,155	233
DMCT	✗	Lobby	47.1	86.4	13,774	12,223	1,136	50.6	89.6	12,574	7,425	720
DMCT	✓	Lobby	69.4	94.5	3,343	7,361	318	69.2	95.1	2,445	7,007	247
DMCT	✗	Office	50.0	89.0	3,287	8,577	591	40.0	85.8	2,849	12,569	735
DMCT	✓	Office	68.0	93.7	1,514	5,625	67	66.8	93.9	1,454	5,304	127
DMCT	✗	Retail	27.7	60.7	79,443	15,788	3,170	30.4	70.7	50,713	20,060	2,667
DMCT	✓	Retail	45.7	85.8	17,795	16,440	1,305	49.4	88.3	15,598	12,756	1,049

Table 6. Tracking performance of each environment on validation split. We compare the detection model trained with and without each domain-specific data. Without any environment-specific data, trackers’ performance drops significantly.

Method	w/Env Training	Env	Without external data					With external data				
			IDF1↑	MOTA↑	FP↓	FN↓	IDs↓	IDF1↑	MOTA↑	FP↓	FN↓	IDs↓
DMCT-TD	✗	Cafe	77.4	95.7	503	6,635	39	76.0	96.8	488	4,885	36
DMCT-TD	✓	Cafe	76.4	96.9	740	4,385	62	74.8	97.1	742	4,119	53
DMCT-TD	✗	Industry	73.8	87.7	7,400	15,661	62	74.2	90.0	7,714	11,039	67
DMCT-TD	✓	Industry	79.0	91.1	7,692	8,947	64	79.4	92.6	8,021	5,812	47
DMCT-TD	✗	Lobby	88.4	96.4	520	6,587	83	82.4	97.2	115	5,419	54
DMCT-TD	✓	Lobby	85.7	96.2	31	7,520	49	86.8	97.3	145	5,303	25
DMCT-TD	✗	Office	85.2	93.7	714	6,420	43	85.9	97.6	884	1,770	38
DMCT-TD	✓	Office	81.3	97.4	787	2,182	42	89.0	98.0	994	1,237	47
DMCT-TD	✗	Retail	56.4	87.7	8,622	21,549	592	57.8	85.9	13,258	21,397	747
DMCT-TD	✓	Retail	58.5	89.6	5,820	19,820	403	65.3	91.3	9,333	12,034	395

Table 7. Tracking performance of each environment on validation split with the top-down detector. We compare the detection model trained with and without each domain-specific data. With the top-down detector, the performance of different models is similar.

is still far from satisfactory in a challenging environment. We believe that more identities are needed to learn more discriminative Re-ID features in these challenging environments.

Env	Generalization		Adaptation		Supervised	
	mAP	R-1	mAP	R-1	mAP	R-1
Cafe	48.82	77.78	63.61	88.01	59.55	87.80
Industry	39.42	65.84	51.39	79.15	44.77	76.26
Lobby	46.08	72.63	60.36	87.43	51.63	82.79
Office	42.89	73.47	58.72	80.64	51.20	76.79
Retail	28.46	49.33	33.25	58.29	31.64	57.43

Table 8. Person re-identification (ReID) performance of each environment on the testing split. We report the performance of three different training settings.

5. Conclusion

In deep learning, high-quality labeled data is fundamental to achieving desired performance in many AI tasks. This is particularly the case for multi-camera multiple people tracking, where trackers’ performance is profoundly impacted by environment settings, *e.g.*, camera angles, back-

grounds, and lighting conditions. In this work, We manage to build the largest multi-camera multiple people tracking dataset with the help of an auto-annotation system, which employs various calibrated depth sensors and RGB sensors to construct a robust 3D tracker and generates reliable multi-camera tracking ground truth. Our dataset offers high-quality, dense annotations for all the captured frames. We study the performance of two real-time trackers and one robust ReID model on the proposed dataset. The results suggest that a large-scale dataset allows the tracking systems and the ReID models to perform better. We believe these findings will benefit the design of real-world tracking systems. For example, for a large chain retailer, where the interior designs are similar across different stores, we can use the auto-annotation system to create a large-scale multi-camera tracking dataset and train an adapted tracker using this dataset to achieve high accuracy for these environments. On the other hand, the experiments also show the challenges of designing a highly accurate multi-camera tracking system in a cluttered and crowded environment, and the baseline methods are far from meeting the accuracy requirements of the demanding applications. We hope our

dataset can encourage more research efforts to be invested in this topic.

References

- [1] Amazon go. <http://amazongo.com>, 2017. 1
- [2] Xavier Alameda-Pineda, Jacopo Staiano, Ramanathan Subramanian, Ligia Maria Batrinca, Elisa Ricci, Bruno Lepri, Oswald Lanz, and Nicu Sebe. SALSA: A novel dataset for multimodal group behavior analysis. *CoRR*, abs/1506.06882, 2015. 2
- [3] Mykhaylo Andriluka, Stefan Roth, and Bernt Schiele. People-tracking-by-detection and people-detection-by-tracking. In *2008 IEEE Conference on computer vision and pattern recognition*, pages 1–8. IEEE, 2008. 2
- [4] Pierre Baqué, François Fleuret, and Pascal Fua. Deep occlusion reasoning for multi-camera multi-target detection. In *Proceedings of the IEEE International Conference on Computer Vision*, pages 271–279, 2017. 2
- [5] Jerome Berclaz, Francois Fleuret, Engin Turetken, and Pascal Fua. Multiple object tracking using k-shortest paths optimization. *IEEE transactions on pattern analysis and machine intelligence*, 33(9):1806–1819, 2011. 2
- [6] Maxim Berman, Hervé Jégou, Andrea Vedaldi, Iasonas Kokkinos, and Matthijs Douze. Multigrain: a unified image embedding for classes and instances. *arXiv preprint arXiv:1902.05509*, 2019. 6
- [7] Keni Bernardin and Rainer Stiefelhagen. Evaluating multiple object tracking performance: the clear mot metrics. *EURASIP Journal on Image and Video Processing*, 2008:1–10, 2008. 1, 2, 5
- [8] Tatjana Chavdarova, Pierre Baqué, Stéphane Bouquet, Andrii Maksai, Cijo Jose, Timur Bagautdinov, Louis Lettry, Pascal Fua, Luc Van Gool, and François Fleuret. Wildtrack: A multi-camera hd dataset for dense unscripted pedestrian detection. In *Proceedings of the IEEE Conference on Computer Vision and Pattern Recognition*, pages 5030–5039, 2018. 2, 5
- [9] Tatjana Chavdarova and François Fleuret. Deep multi-camera people detection. In *2017 16th IEEE International Conference on Machine Learning and Applications (ICMLA)*, pages 848–853. IEEE, 2017. 2
- [10] He Chen, Pengfei Guo, Pengfei Li, Gim Hee Lee, and Gregory Chirikjian. Multi-person 3d pose estimation in crowded scenes based on multi-view geometry. In *European Conference on Computer Vision*, pages 541–557. Springer, 2020. 2
- [11] Weihua Chen, Lijun Cao, Xiaotang Chen, and Kaiqi Huang. An equalized global graph model-based approach for multi-camera object tracking. *IEEE Transactions on Circuits and Systems for Video Technology*, 27(11):2367–2381, 2016. 2
- [12] Afshin Dehghan, Shayan Modiri Assari, and Mubarak Shah. Gmmcp tracker: Globally optimal generalized maximum multi clique problem for multiple object tracking. In *Proceedings of the IEEE conference on computer vision and pattern recognition*, pages 4091–4099, 2015. 2
- [13] Ran Eshel and Yael Moses. Homography based multiple camera detection and tracking of people in a dense crowd. In *2008 IEEE Conference on Computer Vision and Pattern Recognition*, pages 1–8. IEEE, 2008. 2
- [14] James Ferryman and Ali Shahrokni. Pets2009: Dataset and challenge. In *2009 Twelfth IEEE international workshop on performance evaluation of tracking and surveillance*, pages 1–6. IEEE, 2009. 2
- [15] Francois Fleuret, Jerome Berclaz, Richard Lengagne, and Pascal Fua. Multicamera people tracking with a probabilistic occupancy map. *IEEE transactions on pattern analysis and machine intelligence*, 30(2):267–282, 2007. 2
- [16] Lingxiao He, Xingyu Liao, Wu Liu, Xinchun Liu, Peng Cheng, and Tao Mei. Fastreid: A pytorch toolbox for general instance re-identification. *arXiv preprint arXiv:2006.02631*, 2020. 6
- [17] Yuhang He, Xing Wei, Xiaopeng Hong, Weiwei Shi, and Yihong Gong. Multi-target multi-camera tracking by tracklet-to-target assignment. *IEEE Transactions on Image Processing*, 29:5191–5205, 2020. 2
- [18] Martin Hofmann, Daniel Wolf, and Gerhard Rigoll. Hypergraphs for joint multi-view reconstruction and multi-object tracking. In *Proceedings of the IEEE Conference on Computer Vision and Pattern Recognition*, pages 3650–3657, 2013. 2
- [19] Yunzhong Hou and Liang Zheng. Multiview detection with shadow transformer (and view-coherent data augmentation). In *Proceedings of the 29th ACM International Conference on Multimedia*, pages 1673–1682, 2021. 2
- [20] Yunzhong Hou, Liang Zheng, and Stephen Gould. Multiview detection with feature perspective transformation. In *European Conference on Computer Vision*, pages 1–18. Springer, 2020. 2
- [21] Yunzhong Hou, Liang Zheng, Zhongdao Wang, and Shengjin Wang. Locality aware appearance metric for multi-target multi-camera tracking. *arXiv preprint arXiv:1911.12037*, 2019. 2
- [22] Hung-Min Hsu, Yizhou Wang, and Jenq-Neng Hwang. Traffic-aware multi-camera tracking of vehicles based on reid and camera link model. In *Proceedings of the 28th ACM International Conference on Multimedia*, pages 964–972, 2020. 2
- [23] Na Jiang, SiChen Bai, Yue Xu, Chang Xing, Zhong Zhou, and Wei Wu. Online inter-camera trajectory association exploiting person re-identification and camera topology. In *Proceedings of the 26th ACM international conference on Multimedia*, pages 1457–1465, 2018. 2
- [24] Glenn Jocher, Alex Stoken, Ayush Chaurasia, Jirka Borovec, NanoCode012, TaoXie, Yonghye Kwon, Kalen Michael, Liu Changyu, Jiacong Fang, Abhiram V, Laughing, tkianai, yxNONG, Piotr Skalski, Adam Hogan, Jebastin Nadar, imyhxy, Lorenzo Mammana, AlexWang1900, Cristi Fati, Diego Montes, Jan Hajek, Laurentiu Diaconu, Mai Thanh Minh, Marc, albinxavi, fatih, oleg, and wanghaoyang0106. ultralytics/yolov5: v6.0 - YOLOv5n 'Nano' models, Roboflow integration, TensorFlow export, OpenCV DNN support, Oct. 2021. 6
- [25] Cheng-Hao Kuo, Chang Huang, and Ram Nevatia. Inter-camera association of multi-target tracks by on-line learned

- appearance affinity models. In *European Conference on Computer Vision*, pages 383–396. Springer, 2010. 2
- [26] Rainer Kümmerle, Giorgio Grisetti, Hauke Strasdat, Kurt Konolige, and Wolfram Burgard. G2o: A general framework for graph optimization. In *2011 IEEE International Conference on Robotics and Automation*, pages 3607–3613, 2011. 4
- [27] Hei Law and Jia Deng. Cornernet: Detecting objects as paired keypoints. In *Proceedings of the European conference on computer vision (ECCV)*, pages 734–750, 2018. 5
- [28] Joao Paulo Lima, Rafael Roberto, Lucas Figueiredo, Francisco Simoes, and Veronica Teichrieb. Generalizable multi-camera 3d pedestrian detection. In *Proceedings of the IEEE/CVF Conference on Computer Vision and Pattern Recognition*, pages 1232–1240, 2021. 2
- [29] Tsung-Yi Lin, Michael Maire, Serge Belongie, James Hays, Pietro Perona, Deva Ramanan, Piotr Dollár, and C Lawrence Zitnick. Microsoft coco: Common objects in context. In *European conference on computer vision*, pages 740–755. Springer, 2014. 2
- [30] Hao Luo, Youzhi Gu, Xingyu Liao, Shenqi Lai, and Wei Jiang. Bag of tricks and a strong baseline for deep person re-identification. In *Proceedings of the IEEE/CVF Conference on Computer Vision and Pattern Recognition Workshops*, pages 0–0, 2019. 6
- [31] Wenhan Luo, Junliang Xing, Anton Milan, Xiaoqin Zhang, Wei Liu, and Tae-Kyun Kim. Multiple object tracking: A literature review. *Artificial Intelligence*, page 103448, 2020. 1
- [32] Ergys Ristani, Francesco Solera, Roger Zou, Rita Cucchiara, and Carlo Tomasi. Performance measures and a data set for multi-target, multi-camera tracking. In *European conference on computer vision*, pages 17–35. Springer, 2016. 2, 3
- [33] Ergys Ristani and Carlo Tomasi. Features for multi-target multi-camera tracking and re-identification. In *Proceedings of the IEEE conference on computer vision and pattern recognition*, pages 6036–6046, 2018. 2
- [34] Liangchen Song, Jialian Wu, Ming Yang, Qian Zhang, Yuan Li, and Junsong Yuan. Stacked homography transformations for multi-view pedestrian detection. In *Proceedings of the IEEE/CVF International Conference on Computer Vision*, pages 6049–6057, 2021. 2
- [35] Yonatan Tariku Tesfaye, Eyasu Zemene, Andrea Prati, Marcello Pelillo, and Mubarak Shah. Multi-target tracking in multiple non-overlapping cameras using constrained dominant sets. *arXiv preprint arXiv:1706.06196*, 2017. 2
- [36] Hanyue Tu, Chunyu Wang, and Wenjun Zeng. Voxelpose: Towards multi-camera 3d human pose estimation in wild environment. In *Proceedings of the European Conference on Computer Vision (ECCV)*, pages 197–212. Springer, 2020. 2, 6
- [37] Minh Phuoc Vo, Ersin Yumer, Kalyan Sunkavalli, Sunil Hadap, Yaser A Sheikh, and Srinivasa G Narasimhan. Self-supervised multi-view person association and its applications. *IEEE transactions on pattern analysis and machine intelligence*, 2020. 2
- [38] Jiuqing Wan and Liu Li. Distributed optimization for global data association in non-overlapping camera networks. In *2013 Seventh International Conference on Distributed Smart Cameras (ICDSC)*, pages 1–7. IEEE, 2013. 2
- [39] Xiaolong Wang, Ross Girshick, Abhinav Gupta, and Kaiming He. Non-local neural networks. In *Proceedings of the IEEE conference on computer vision and pattern recognition*, pages 7794–7803, 2018. 6
- [40] Longhui Wei, Shiliang Zhang, Wen Gao, and Qi Tian. Person transfer gan to bridge domain gap for person re-identification. In *Proceedings of the IEEE conference on computer vision and pattern recognition*, pages 79–88, 2018. 2, 6
- [41] Longyin Wen, Zhen Lei, Ming-Ching Chang, Honggang Qi, and Siwei Lyu. Multi-camera multi-target tracking with space-time-view hyper-graph. *International Journal of Computer Vision*, 122(2):313–333, 2017. 2
- [42] Yuanlu Xu, Xiaobai Liu, Yang Liu, and Song-Chun Zhu. Multi-view people tracking via hierarchical trajectory composition. In *Proceedings of the IEEE Conference on Computer Vision and Pattern Recognition*, pages 4256–4265, 2016. 2
- [43] Yuhao Xu and Jiakui Wang. A unified neural network for object detection, multiple object tracking and vehicle re-identification. *arXiv preprint arXiv:1907.03465*, 2019. 2
- [44] Quanzeng You and Hao Jiang. Action4d: Online action recognition in the crowd and clutter. In *Proceedings of the IEEE/CVF Conference on Computer Vision and Pattern Recognition*, pages 11857–11866, 2019. 1, 4
- [45] Quanzeng You and Hao Jiang. Real-time 3d deep multi-camera tracking. *arXiv preprint arXiv:2003.11753*, 2020. 2, 5, 6
- [46] Amir Roshan Zamir, Afshin Dehghan, and Mubarak Shah. Gmcp-tracker: Global multi-object tracking using generalized minimum clique graphs. In *European conference on computer vision*, pages 343–356. Springer, 2012. 2
- [47] Shu Zhang, Elliot Staudt, Tim Faltemier, and Amit K Roy-Chowdhury. A camera network tracking (camnet) dataset and performance baseline. In *2015 IEEE Winter Conference on Applications of Computer Vision*, pages 365–372. IEEE, 2015. 2
- [48] Yifu Zhang, Chunyu Wang, Xinggang Wang, Wenyu Liu, and Wenjun Zeng. Voxeltrack: Multi-person 3d human pose estimation and tracking in the wild. *arXiv preprint arXiv:2108.02452*, 2021. 1, 2
- [49] Yifu Zhang, Chunyu Wang, Xinggang Wang, Wenjun Zeng, and Wenyu Liu. Fairmot: On the fairness of detection and re-identification in multiple object tracking. *International Journal of Computer Vision*, pages 1–19, 2021. 6
- [50] Liang Zheng, Yi Yang, and Alexander G Hauptmann. Person re-identification: Past, present and future. *arXiv preprint arXiv:1610.02984*, 2016. 2, 5